

This is the accepted manuscript made available via CHORUS. The article has been published as:

Reinvestigation of the level structures of the ${}^{49}\text{N}$ isotones

and ${}^{89}\text{Zr}$

and ${}^{91}\text{Mo}$

Zhen Ren, Jing-Bin Lu, Gao-Long Zhang, Yi-Heng Wu, Tian-Jiao Gao, Ke-Yan Ma, Zhen Huang, Guang-Xin Zhang, Ming-Li Wang, Shi-Peng Hu, Hui-Bin Sun, Huan-Qiao Zhang, D. Testov, P. R. John, J. J. Valiente-Dobon, A. Goasduff, M. Siciliano, F. Galtarossa, D. Mengoni, and D. Bazzacco

Phys. Rev. C **106**, 024323 — Published 19 August 2022

DOI: [10.1103/PhysRevC.106.024323](https://doi.org/10.1103/PhysRevC.106.024323)

Reinvestigation of the level structures of the N=49 isotones ^{89}Zr and ^{91}Mo

Zhen Ren¹, Jing-Bin Lu^{1,*}, Gao-Long Zhang^{2,†}, Yi-Heng Wu³, Tian-Jiao Gao¹, Ke-Yan Ma¹, Zhen Huang², Guang-Xin Zhang^{4,5}, Ming-Li Wang², Shi-Peng Hu⁶, Hui-Bin Sun⁶, Huan-Qiao Zhang⁷, D. Testov⁸, P. R. John^{4,5}, J. J. Valiente-Dobon⁹, A. Goasduff⁴, M. Siciliano^{9,10}, F. Galtarossa⁹, D. Mengoni^{4,5}, and D. Bazzacco⁵

¹College of Physics, Jilin University, Changchun 130012, China

²School of Physics, Beihang University, Beijing 100191, China

³School of Electronic Engineering and Intelligent Manufacturing, Anqing Normal University, Anqing 246133, China

⁴Dipartimento di Fisica, Università di Padova, 35131 Padua, Italy

⁵Istituto Nazionale di Fisica Nucleare, Sezione di Padova, Padua, Italy

⁶College of Physics and Optoelectronic Engineering, Shenzhen University, Shenzhen 518060, China

⁷China Institute of Atomic Energy, Beijing 102413, China

⁸Extreme Light Infrastructure-Nuclear Physics, IFIN-HH, Bucharest-Magurele, 077125, Romania

⁹INFN, Laboratori Nazionali di Legnaro, Legnaro(Padova), Italy

¹⁰Physics Division, Argonne National Laboratory, Lemont-IL, 60439, USA

(Dated: August 4, 2022)

Excited states of ^{89}Zr and ^{91}Mo have been investigated using the fusion reaction $^6\text{Li}+^{89}\text{Y}$ at beam energy of 34 MeV. Based on new experimental data, about 16 (13) new transitions have been added to the level scheme of ^{89}Zr (^{91}Mo). The level structures are investigated in the framework of the spherical-basis shell model using the effective interactions JUN45 and GWBXXG. Reasonable agreement is obtained between the experimental results and the calculations. The calculated results indicate the newly proposed states are characterized by proton excitations from the $1f_{5/2}$, $2p_{3/2}$, $2p_{1/2}$ orbits to the high-j $1g_{9/2}$ orbit. The systematic features of low lying states in the N=49 isotones are discussed.

I. INTRODUCTION

The level schemes of nuclei in the $Z\sim 40$, $N\sim 50$ region have attracted considerable attention in both experiments and theories for many years [1–12]. Studies of nuclei in this region can provide a testing ground for the interactions developed for the shell model. These nuclei are suitable objects to understand the mechanism of particle-hole excitations. It is worth to focus on the excitation of valence nucleons across the $Z=38$ ($Z=40$) subshell and $N=50$ shell and research their profound impact on generating high spin states [12–16]. The nuclei with $N=49$ have a neutron hole in the $g_{9/2}$ orbit, which are ideal candidates to study the origin of the high spin states. The isotones such as ^{88}Y , ^{90}Nb , ^{92}Tc , ^{93}Ru , have been studied using different fusion evaporation reactions [4, 11, 17–22]. In this work, we investigate the level structures of two isotones, ^{89}Zr and ^{91}Mo .

The level scheme of ^{89}Zr , has been studied using different reactions, such as $^{88}\text{Sr}(\alpha,3n)$, $^{74}\text{Ge}(^{18}\text{O},3n)$, $^{76}\text{Ge}(^{18}\text{O},5n)$ and $^{80}\text{Se}(^{13}\text{C},4n)$ [11, 23, 24]. In Ref. [25], the known level scheme was extended to the $49/2^-$ state at 12256 keV. Spectroscopy of high spin states in ^{91}Mo was established by $^{90}\text{Zr}(\alpha,3n)$, $^{66}\text{Zn}(^{28}\text{Si},2pn)$ and $^{63}\text{Cu}(^{31}\text{P},2np)$ [20, 23, 26] and had been observed up to an excitation energy of $E_x\sim 10$ MeV. Though considerable information for high spin states in both nuclei is available, the middle-low excited states are relatively

scarce. To provide more information on the level structures of N=49 nuclei, we have reinvestigated ^{89}Zr and ^{91}Mo .

We have organized the article in six sections. In Sec. II, the experimental details are introduced. The experimental results and new level schemes for ^{89}Zr and ^{91}Mo are shown in Sec. III. Discussions within the framework of shell model are presented in Sec. IV. The systematic features of ^{89}Zr and ^{91}Mo with neighboring nuclei are discussed in Sec. V. Finally, we take a brief summary about the present work.

II. EXPERIMENTAL DETAILS

Excited states of ^{89}Zr and ^{91}Mo were populated using the $^{89}\text{Y}(^6\text{Li},2p4n)^{89}\text{Zr}$, $^{89}\text{Y}(^6\text{Li},4n)^{91}\text{Mo}$ reactions at a beam energy of 34 MeV. The $^6\text{Li}^{3+}$ beam with an average intensity of 1.0 enA was delivered by Tandem-XTU accelerator at LNL-INFN in Italy. The target consists of $550\ \mu\text{g}/\text{cm}^2$ ^{89}Y evaporated on a $340\ \mu\text{g}/\text{cm}^2$ ^{12}C backing. The ^{12}C foil was used to stop all the fusion-evaporation residues [27]. The deexcitation γ rays were detected by the GALILEO array comprising of 25 Compton-suppressed high-purity germanium (BGO-HPGe) detectors [28]. The detectors were arranged at four different angles with respect to the beam axis. Ten were placed at 90. Others were at 119, 129 and 152, where five detectors were placed under each angle. The γ ray spectra measured by different rings of GALILEO were shown in Ref. [27]. We could see that the line shapes of strong γ ray lines originating from fusion evap-

* 1)E-mail:ljb@jlu.edu.cn

† 2)E-mail:zgl@buaa.edu.cn

oration reactions did not show a Doppler-shifted component, which confirmed that the recoiling nuclei were in fact stopped. The data on ^{89}Zr and ^{91}Mo presented in this work were determined in an experiment where the EUCLIDES 4π Si-ball array was employed [29]. However, the main subject of this experiment was to investigate the influence of breakup and transfer of weakly bound projectiles on the fusion process using particle- γ coincidences [30]. The fusion-evaporation reactions for the population of ^{89}Zr and ^{91}Mo are a by-product of the aforementioned reaction study. No particle- γ analysis was done in our work mainly due to two reasons. For the first one, no charged particles were emitted in the reaction $^{89}\text{Y}(^6\text{Li},4n)^{91}\text{Mo}$. And the second one is low statistics for ^{89}Zr . A total of 1.4×10^7 γ - γ coincidence events were recorded and sorted into a two-dimensional symmetric E_γ - E_γ matrix for subsequent offline analysis.

In order to determine the multiplicities of the newly observed γ rays and the spins of the related states, two asymmetric coincidence matrices were constructed, with one axis (y axis) using the γ rays detected at all angles, and the other axis (x axis) using those detected at 152 and those detected at 90, respectively. Assuming that γ_1 and γ_2 are the cascading transitions in the same nucleus, the angular distribution asymmetry ratios is defined as $R_{ADO} = I_{\gamma_1}(152)/I_{\gamma_1}(90)$, where $I_{\gamma_1}(152$ or $90)$ represents the intensity of γ_1 rays collected by the detectors at 152 or 90 in the coincidence spectra gated on γ_2 rays measured by all detectors [31, 32]. By calculating the ADO ratio of γ rays with known multipolarity in ^{92}Mo , ^{92}Nb , ^{91}Mo , ^{89}Zr and ^{91}Nb , typical ADO ratios for stretched quadrupole or $\Delta I=0$ dipole or largely mixed $\Delta I=1$ transitions and stretched pure dipole transitions are found to be 1.6 and 0.9, respectively, as shown in Fig. 1. Hence, uncertainties exist for the spin and parity assignments based on the ADO ratio analysis. In these cases, we can consider the crossover or parallel transitions and their branching ratios as supplementary arguments for the spin and parity assignments.

III. EXPERIMENTAL RESULTS

A. Results for ^{89}Zr

Based on the present data, 8 new levels and 16 new transitions belonging to ^{89}Zr were observed. The latest level scheme is shown in Fig. 2, and new transitions (levels) are marked in red. Typical prompt γ - γ coincidence spectra for ^{89}Zr are shown in Figs. (3-5). The placement of decaying γ rays was based on the relative intensities, energy sums and coincidence relationships. The spin assignments to the states have been made based on the ADO ratios. The γ ray energies, relative intensities, ADO ratios and spin assignments are listed in Table I. In the following, the extensions and corrections for the level structure compared with the previous work will be discussed.

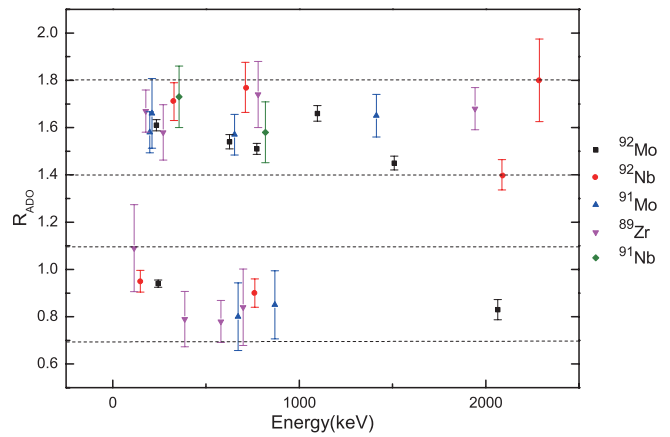


FIG. 1. Representative ADO ratios in ^{92}Mo , ^{92}Nb , ^{91}Mo , ^{89}Zr and ^{91}Nb . Typical ADO ratios for stretched quadrupole or $\Delta I=0$ dipole or largely mixed $\Delta I=1$ transitions and stretched pure dipole transitions are found to be 1.6 and 0.9, respectively.

In group A, the 332.0 keV transition was placed above the 2120.7 keV level in Refs. [11, 24]. It is also coincident with the 207.0 keV transition from the analysis of present data. Several new transitions with energies of 105.1, 341.5, 371.0, 447.0 and 476.5 keV were identified. Figure 3 demonstrates the spectra gated on the 332.0, 207.0 and 177.2 keV transitions. As shown in Fig. 3, the new 105.1, 341.5, 371.0, 447.0 and 476.5 transitions are visible in the coincidence spectrum gated on the 177.2 keV transition and the 105.1, 332.0, 341.5 keV transitions are observed from the 207.0 keV γ ray coincidence spectrum. Energy of the 341.5 keV γ ray is 9.5 keV more than 332.0 keV. As to the 371.0 keV γ ray, its energy is 29.5 keV larger than 341.5 keV. The difference between the 476.5 and 447 keV γ rays is also 29.5 keV. There were two transitions with energies of 8.4 and 29.2 keV, reported in Ref. [24], corresponding to the energies of 9.5 and 29.5 keV in our work. However, we could not observe them due to the fact that such extremely low γ ray energies are typically below the energy threshold of the γ ray detectors. Based on the coincidence relationships and energy difference mentioned above, two new levels, 2491.7 and 2597.2 keV, are constructed, and the 332.0 keV transition is placed above the $17/2^-$ state at 2160.0 keV. Besides, the 621.5 and 591.6 keV γ rays are added on account of the same reasons. It is noteworthy that the energy of the 746.4 keV transition is close to the previously known transition, 748 keV [11]. However, we confirm that the two transitions are different because in our data, the 746.4 keV γ ray is only coincident with the 177.2, 207.0, 1943.2 and 2020.7 keV transitions. Comparing with Ref. [11], all transitions except the 214.6 keV γ ray from the $29/2^-$ state are below the sensitivity limit in our work due to the efficiency and the achievable statistics.

As for transitions in group B, the new transitions with 787.5, 902.5, 1523.7, 1638.7 keV belonging to ^{89}Zr are

found to be in coincidence with the 270.9, 780.1 and 1943.2 keV transitions, but not with the 1739.8 and 580.3 keV transitions populating the $21/2^+$ state (2994.2 keV level). As shown in Figs. 4-5, the four new transitions

TABLE I. γ -ray energies, relative intensities, measured ADO ratios, initial and final level energies, and initial as well as final spins of transitions in ^{89}Zr .

E_γ ^{a b}	I_γ	R_{ADO}	E_i ^b	E_f ^b	J_i^π	J_f^π
keV			keV	keV		
105.1*	2.31(17)	1.21(30)	2597.2*	2491.7*	(17/2 ⁻)	(15/2 ⁻)
115.3	4.51(25)	1.09(18)	3109.5	2994.2	19/2 ⁺	21/2 ⁺
177.2	117.4(28)	1.67(9)	2120.7	1943.2	13/2 ⁻	13/2 ⁺
207.0	8.94(48)	0.85(17)	2150.2	1943.2	15/2 ⁻	13/2 ⁺
214.6	3.73(29)	0.98(29)	6239.9	6025.3	29/2 ⁻	27/2 ⁺
222.2*	0.78(10)		3897.0*	3674.5*	(21/2 ⁺)	(19/2 ⁺)
270.9	65.4(18)	1.59(12)	2994.2	2723.3	21/2 ⁺	17/2 ⁺
322.4*	1.10(10)		3897.0*	3574.5	(21/2 ⁺)	23/2 ⁺
332.0	16.00(74)	0.77(8)	2491.7*	2160.0	(15/2 ⁻)	17/2 ⁻
341.5*	2.97(22)	1.44(35)	2491.7*	2150.2	(15/2 ⁻)	15/2 ⁻
358.3*	7.82(49)	0.78(19)	3187.6*	2829.3	(17/2 ⁺)	(15/2 ⁺)
371.0*	2.35(18)	1.03(26)	2491.7*	2120.7	(15/2 ⁻)	13/2 ⁻
386.5	12.23(47)	0.79(12)	3109.5	2723.3	19/2 ⁺	17/2 ⁺
447.0*	2.72(21)	1.17(29)	2597.2*	2150.2	(17/2 ⁻)	15/2 ⁻
476.5*	5.88(35)	1.38(25)	2597.2*	2120.7	(17/2 ⁻)	13/2 ⁻
532.2	4.26(42)	0.99(28)	6025.3	5493.6	27/2 ⁺	25/2 ⁻
563.3	8.56(57)	1.66(26)	2723.3	2160.0	17/2 ⁺	17/2 ⁻
580.3	30.6(14)	0.78(9)	3574.5	2994.2	23/2 ⁺	21/2 ⁺
587.3	3.38(50)	0.73(25)	6827.2	6239.9	31/2 ⁻	29/2 ⁻
591.6*	4.46(30)	0.78(16)	2741.8*	2150.2	(17/2 ⁻)	15/2 ⁻
621.5*	5.76(36)	1.46(29)	2741.8*	2120.7	(17/2 ⁻)	13/2 ⁻
640.9	4.44(30)	0.81(24)	5374.7	4733.8	27/2 ⁺	25/2 ⁺
673.3	1.83(24)		7500.5	6827.2	33/2 ⁻	31/2 ⁻
699.3	11.26(61)	0.84(16)	4273.8	3574.5	25/2 ⁺	23/2 ⁺
746.4*	4.95(34)	1.11(25)	2896.6*	2150.2	(17/2 ⁻)	15/2 ⁻
767.2	18.91(91)	0.66(9)	2927.3	2160.0	19/2 ⁻	17/2 ⁻
780.1	100	1.74(14)	2723.3	1943.2	17/2 ⁺	13/2 ⁺
787.5*	2.90(24)	0.90(33)	3897.0*	3109.5	(21/2 ⁺)	19/2 ⁺
790.1	4.59(32)	0.76(20)	3717.6	2927.3	21/2 ⁻	19/2 ⁻
806.0	3.31(28)	0.89(26)	4522.9	3717.6	23/2 ⁻	21/2 ⁻
886.1	15.91(89)	0.69(17)	2829.3	1943.2	(15/2 ⁺)	13/2 ⁺
902.5*	2.53(24)		3897.0*	2994.2	(21/2 ⁺)	21/2 ⁺
951.2*	2.11(23)	0.49(20)	3674.5*	2723.3	(19/2 ⁺)	17/2 ⁺
970.1	1.57(18)		5493.6	4522.9	25/2 ⁻	23/2 ⁻
1014.5	3.05(65)		5748.3	4733.8	27/2 ⁺	25/2 ⁺
1159.3	1.55(21)		4733.8	3574.5	25/2 ⁺	23/2 ⁺
1291.5	1.98(21)		6025.3	4733.8	27/2 ⁺	25/2 ⁺
1523.7*	1.80(23)		4633.2*	3109.5		19/2 ⁺
1557.6	6.72(47)	1.38(34)	3717.6	2160.0	21/2 ⁻	17/2 ⁻
1638.7*	3.18(33)		4633.2*	2994.2		21/2 ⁺
1739.8	9.23(60)	1.47(40)	4733.8	2994.2	25/2 ⁺	21/2 ⁺
1776.0	3.62(34)		5493.6	3717.6	25/2 ⁻	21/2 ⁻
1943.2	242.4(42)	1.68(9)	1943.2	0	13/2 ⁺	9/2 ⁺
2120.7	65.5(43)		2120.7	0	13/2 ⁻	9/2 ⁺
2174.0	1.26(24)		5748.3	3574.5	27/2 ⁺	23/2 ⁺

^a The uncertainty in strong γ -ray energies is about 0.3 keV; for weak γ -ray energies, it is about 0.6 keV.

^b The asterisks denote newly identified γ -ray transitions and excited states.

can be observed from the γ ray coincidence spectrum gated on 1943.2 keV transitions and the known transitions can also be observed from the 787.5 and 902.5 keV. In addition, after careful analysis, the new 787.5 and 1523.7 keV transitions are found to be in coincidence with the known 386.5 and 115.3 keV transitions and they are not coincident with each other. From analysis of coincidence relationship and energy sum relationships, these transitions are placed on top of the $19/2^+$ (3109.5 keV level) and $21/2^+$ (2994.2 keV level) states as shown in Fig. 2.

When it comes to group C, the 886.1 keV γ ray found by the reaction $^{88}\text{Sr}(\alpha,3n\gamma)$ [33] is confirmed in the current work. A new transition, 358.3 keV, is found to be coincident with the 1943.2 and 886.1 keV transitions and placed above the 2829.3 keV level.

B. Results for ^{91}Mo

The level structure of ^{91}Mo from the present experiment is shown in Fig. 6. Typical prompt γ - γ coincidence spectra for ^{91}Mo are shown in Fig. 8. The γ ray energies, relative intensities, ADO ratios and spin assignments are listed in Table II.

In group A, the 1272.4 and 1471.6 keV γ rays are observed in the spectrum gated on the 1413.6 keV transition, while the 1272.4 γ ray is also coincident with the 199.1 keV γ ray. Considering the difference between the γ ray lines at 1471.6 keV and 1272.4 keV and the related γ ray intensities, there are supposed to be two 199.1 keV γ rays.

A. Nilsson and M. Grecescu reported a 211.7 keV transition decaying into the 2067 keV level in Ref. [23] and we observe it in our data. From the analysis of present data, a new transition of energy 346.5 keV is observed to feed the level 2278.3 keV as shown in group B. Two new levels with energies of 2216.6, 2291.7 keV are constructed based on the coincidence relationships and especially energy sums. A new 327.0 keV γ ray is found to be in coincidence with the 199.1, 653.5 and 1413.6 keV transitions as can be seen in Fig. 8(c). Two transitions with energies of 971.9 and 1132.0 keV have been observed as well. In addition, it can be noted that there are two Doppler-shifted peaks in Fig. 8(b), which correspond to the 718 and 1021 keV γ rays in ^{10}B . Both transitions are coincident with the 414 keV γ ray [35]. Excited states of ^{10}B were populated through the reaction between the ^6Li beam and the ^{12}C foil.

IV. SHELL MODEL CALCULATIONS

A. Results for ^{89}Zr

The level structure of ^{89}Zr shows the characteristics of particle-hole excitations as can be seen in Ref. [11]. To interpret the spectrum of ^{89}Zr in the present work,

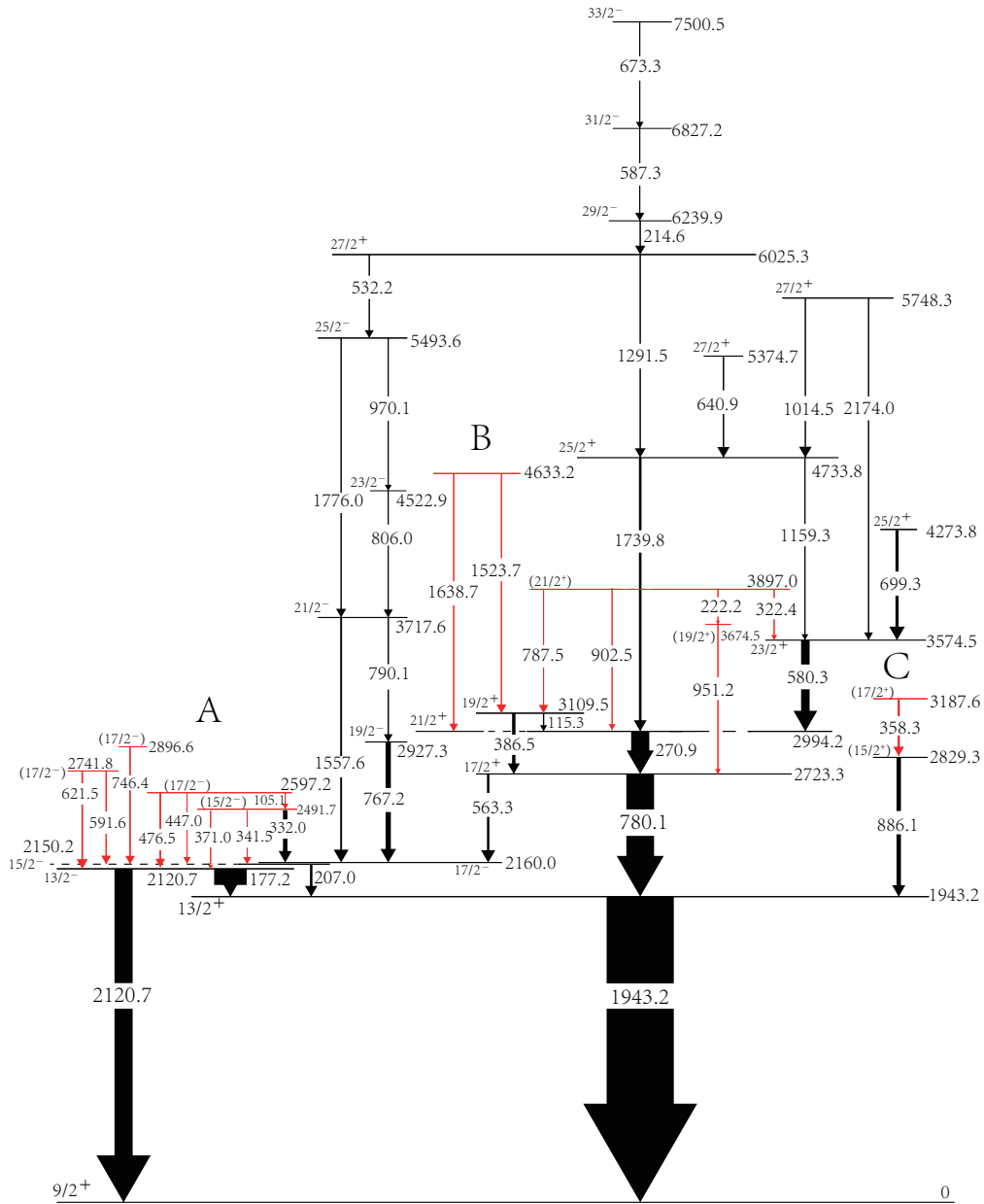


FIG. 2. Level scheme of ^{89}Zr established in the present work. New transitions and levels are marked in red. The arrow widths relate to the observed γ -ray intensities.

we performed the calculations within the 28-50 valence space including four orbits ($1f_{5/2}$, $2p_{3/2}$, $2p_{1/2}$, $1g_{9/2}$). The JUN45 interaction developed by Honma *et al.* [36] was used. The single-particle energies are set as -9.8280, -8.7087, -7.8388 and -6.2617 MeV for the $1f_{5/2}$, $2p_{3/2}$, $2p_{1/2}$ and $1g_{9/2}$ orbits, respectively. The shell model calculations were performed using the NushellX [37]. No truncations were applied to this model space. In Fig. 7, the comparison of the experimental excitation energies with the results predicted by shell-model calculations is shown. It is obvious that the experimental results are well reproduced by the calculations. The dominant partitions of wave functions are listed in Table III.

The ground state $9/2^+$ primarily stems from the $\pi(p_{1/2}^2 g_{9/2}^0) \otimes \nu(p_{1/2}^2 g_{9/2}^9)$ and $\pi(p_{1/2}^0 g_{9/2}^2) \otimes \nu(p_{1/2}^2 g_{9/2}^9)$ configurations. The low lying states from $13/2^+$ to the $25/2_1^+$ state are well described by $\pi(f_{5/2}^6 p_{3/2}^4 p_{1/2}^0 g_{9/2}^2) \otimes \nu(p_{1/2}^2 g_{9/2}^9)$. The experimental values of $B(E2; 13/2^+ \rightarrow 9/2^+)$, $B(E2; 17/2_1^+ \rightarrow 13/2^+)$ and $B(E2; 21/2_1^+ \rightarrow 17/2_1^+)$ are 1.17(18), 7.5(21) and 3.05(16) in W.u. [33]. We have calculated $B(E2)$ values for these E2 transitions, and our calculations give the results 2.46, 6.02 and 2.16 in W.u., respectively. Proton excitations across the $Z=38$ subshell play an important role in generating states from the $25/2_2^+$ to

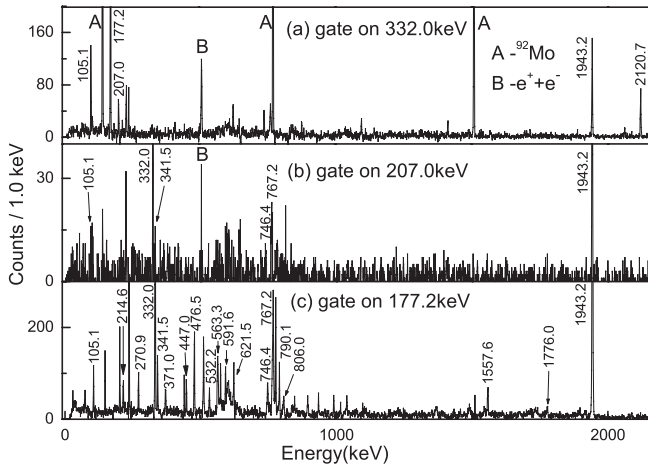


FIG. 3. Spectra of γ rays for ^{89}Zr , gated on (a) 332.0 keV; (b) 207.0 keV; (c) 177.2 keV. Appearance of peaks labeled A is influenced by the 329 keV transition in ^{92}Mo [34].

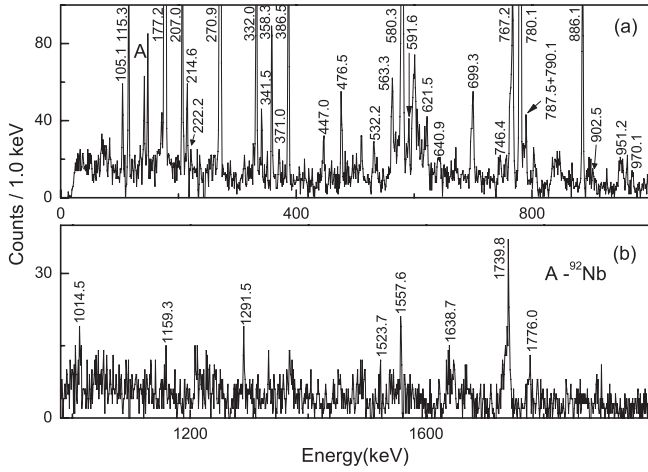


FIG. 4. Spectra of γ rays for ^{89}Zr , gated on 1943.2 keV.

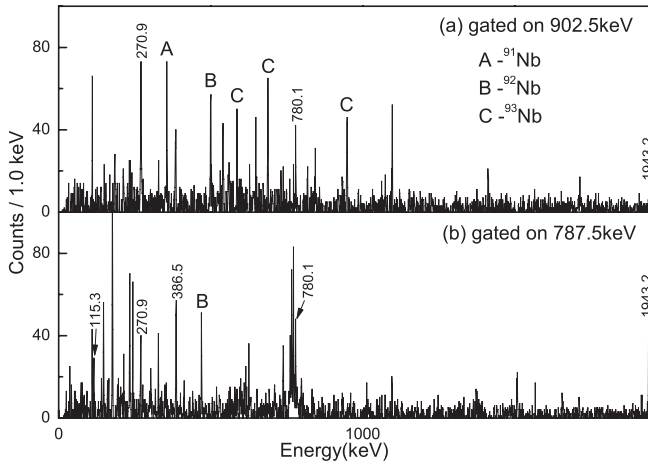


FIG. 5. Spectra of γ rays for ^{89}Zr , gated on (a) 902.5 keV; (b) 787.5 keV. Peaks not labeled are not coincident with other transitions in ^{89}Zr and the coincidence relationship was not reported in other nuclei.

the third $27/2^+$. The $25/2^+$, $27/2^+$, $27/2^+$ and $27/2^+$ have the configuration $\pi(f_{5/2}^6 p_{3/2}^4 p_{1/2}^2 g_{9/2}^2) \otimes \nu(p_{1/2}^2 g_{9/2}^9)$, mixed with $\pi(f_{5/2}^6 p_{3/2}^3 p_{1/2}^2 g_{9/2}^2) \otimes \nu(p_{1/2}^2 g_{9/2}^9)$. We are not able to determine the spin of the 4633.2 keV level due to low statistics, which should be noted. Transitions decaying from this level feed into the $19/2^+$ and $21/2^+$ states and its energy coincides with the calculated level $23/2^+$. Hence, this state could possibly have spin and parity $23/2^+$. The state is predicted to contain both the $\pi(f_{5/2}^6 p_{3/2}^3 p_{1/2}^2 g_{9/2}^2) \otimes \nu(p_{1/2}^2 g_{9/2}^9)$ and $\pi(f_{5/2}^6 p_{3/2}^4 p_{1/2}^2 g_{9/2}^2) \otimes \nu(p_{1/2}^2 g_{9/2}^9)$ configuration components.

As for the negative parity states, proton excitation from the $p_{1/2}$ orbit to $g_{9/2}$ has a substantial contribution to the states from $13/2^-$ to $19/2^-$ except $17/2_3^-$. The $17/2_3^-$ state primarily arises from the configuration $\pi(f_{5/2}^6 p_{3/2}^3 p_{1/2}^2 g_{9/2}^1) \otimes \nu(p_{1/2}^2 g_{9/2}^9)$. It is worth noting that the 2741.8 keV level is not reproduced by the calculations. The state may be generated by the same reason as the 2597.2 keV level, dominated by $\pi(p_{1/2}^1 g_{9/2}^2) \otimes \nu(p_{1/2}^2 g_{9/2}^9)$. The $21/2^-$ and $23/2^-$ states

TABLE II. γ -ray energies, relative intensities, measured ADO ratios, initial and final level energies, and initial as well as final spins of transitions in ^{91}Mo .

E_γ ^{a,b} keV	I_γ	R_{ADO}	E_i ^b keV	E_f ^b keV	J_i^π	J_f^π
61.1*	2.29(30)		2278.3	2216.6*	$17/2^-$	$(15/2^+)$
149.7*	2.45(14)	0.81(30)	2216.6*	2067.1	$(15/2^+)$	$17/2^+$
199.1	65.08(40)	1.58(9)	2266.2	2067.1	$21/2^+$	$17/2^+$
199.1*			2885.2*	2686.0*		
211.2	23.49(52)	1.66(15)	2278.3	2067.1	$17/2^-$	$17/2^+$
264.0	1.02(9)		3806.5	3542.4	$25/2^+$	$25/2^+$
284.1	0.69(7)	1.00(25)	5238.0	4953.9	$31/2^+$	$29/2^+$
327.0*	4.63(24)	1.14(16)	2593.2*	2266.2	$(19/2^+)$	$21/2^+$
333.0*	1.14(14)		2624.7*	2291.7*	$(17/2^-)$	$(15/2^-)$
346.5*	2.17(15)	1.42(34)	2624.7*	2278.3	$(17/2^-)$	$17/2^-$
408.6*	3.93(30)	0.84(22)	2624.7*	2216.6*	$(17/2^-)$	$(15/2^+)$
531.3	4.09(24)	0.52(13)	4337.8	3806.5	$27/2^+$	$25/2^+$
605.0	8.42(43)	0.82(21)	3542.4	2937.4	$25/2^+$	$23/2^+$
616.1	1.70(17)	1.13(25)	4953.9	4337.8	$29/2^+$	$27/2^+$
653.5	86.70(56)	1.57(9)	2067.1	1413.6	$17/2^+$	$13/2^+$
671.2	20.55(57)	0.80(14)	2937.4	2266.2	$23/2^+$	$21/2^+$
803.0*	7.81(40)	0.87(17)	2216.6*	1413.6	$(15/2^+)$	$13/2^+$
869.1	7.00(35)	0.85(14)	3806.5	2937.4	$25/2^+$	$23/2^+$
878.1*	5.43(34)	0.98(22)	2291.7*	1413.6	$(15/2^-)$	$13/2^+$
971.9*	0.71(8)		3238.1*	2266.2		$21/2^+$
1132.0*	1.03(15)		3199.1*	2067.1		$17/2^+$
1272.4*	0.85(16)		2686.0*	1413.6		$13/2^+$
1413.6	100	1.65(9)	1413.6	0	$13/2^+$	$9/2^+$
1471.6*	0.96(18)		2885.2*	1413.6		$13/2^+$
2176.3	1.31(21)		4442.5	2266.2	$25/2^+$	$21/2^+$

^a The uncertainty in strong γ -ray energies is about 0.3 keV; for weak γ -ray energies, it is about 0.6 keV.

^b The asterisks denote newly identified γ -ray transitions and excited states.

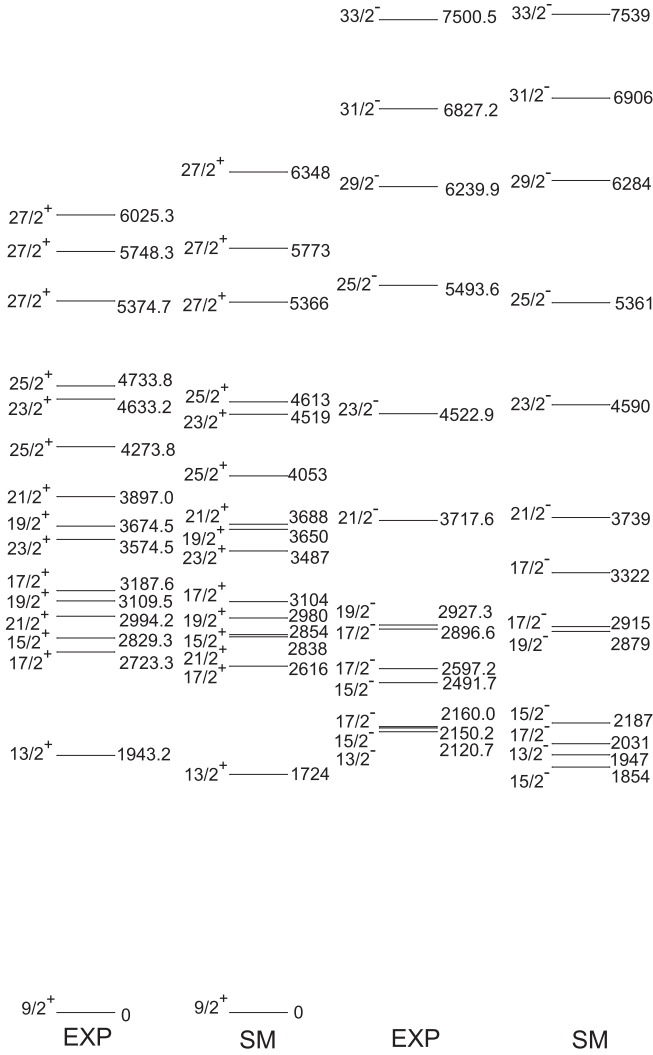


FIG. 7. Comparison of the calculated levels and the experimental levels of ^{89}Zr .

GWBXG interaction are from bare G matrix of the H7B potential [38]. For the present G -matrix effective interaction, the 65 TMBEs for proton orbitals are replaced with the values reported in Ref. [39]. The TMBEs between the $\pi(2p_{1/2}, 1g_{9/2})$ and the $\nu(2d_{5/2}, 3s_{1/2})$ orbitals and that between the $\pi(2p_{1/2}, 1g_{9/2})$ and the $\nu(2p_{1/2}, 1g_{9/2})$ orbitals are replaced with the values obtained from the work of Gloeckner [40] and Serduke *et al.* [41], respectively. Due to the computational difficulties, truncations were employed. At most four protons were allowed to across the $Z=38$ subshell. Considering the neutron excitation across the $N=50$ core to the next major shell occurs in high angular momentum states ($J \geq 35\hbar/2$) [20], neutrons were restricted in the $2p_{1/2}$ and $1g_{9/2}$ orbits. The comparison of the experimental levels with the predictions of shell model calculations is shown in Fig. 9, and the detailed calculation results are presented in Table IV. We can see that the calculations have good agreement with the experimental results.

It can be seen that the low lying states up to $25/2_1^+$ are well reproduced, mainly generating by the $\pi(p_{1/2}^2 g_{9/2}^2) \otimes \nu(p_{1/2}^2 g_{9/2}^9)$ and $\pi(p_{1/2}^0 g_{9/2}^4) \otimes \nu(p_{1/2}^2 g_{9/2}^9)$ configurations. We fail to determine the ADO ratio of the 1132.0 keV γ ray because of low statistics. Considering that it decays into the $17/2^+$ state and the calculational results, the 3199.1 level possibly has spin and parity $19/2^+$ and mainly arises from $\pi(p_{1/2}^2 g_{9/2}^2) \otimes \nu(p_{1/2}^2 g_{9/2}^9)$ and $\pi(p_{1/2}^0 g_{9/2}^4) \otimes \nu(p_{1/2}^2 g_{9/2}^9)$. The promotion of a proton from the $f_{5/2}$ to the $p_{1/2}$ orbit and a $p_{1/2}$ proton pair to $g_{9/2}$ has significant impact on generating the $25/2_2^+$, $25/2_3^+$, $27/2^+$, $29/2^+$ and $31/2^+$ states.

For the negative parity states, the $15/2^-$ and $17/2_1^-$ are characterized by proton excitation

TABLE III. Main components of the wave functions and their partitions in ^{89}Zr . $\pi \otimes \nu$ represents $\pi(f_{5/2} p_{3/2} p_{1/2} g_{9/2}) \otimes \nu(f_{5/2} p_{3/2} p_{1/2} g_{9/2})$.

J^π	E_{exp}	E_{cal}	Wave function	Partitions
\hbar	keV	keV	$\pi \otimes \nu$	
$9/2^+$	0	0	$6420 \otimes 6429$	36.4%
			$6402 \otimes 6429$	20.0%
$13/2^+$	1943.2	1799	$6402 \otimes 6429$	48.8%
$15/2^+$	2829.3	2854	$6402 \otimes 6429$	56.2%
$17/2_1^+$	2723.3	2616	$6402 \otimes 6429$	54.9%
$17/2_2^+$	3187.6	3104	$6402 \otimes 6429$	53.2%
$19/2_1^+$	3109.5	2980	$6402 \otimes 6429$	55.7%
$19/2_2^+$	3674.5	3650	$6402 \otimes 6429$	53.0%
$21/2_1^+$	2994.2	2838	$6402 \otimes 6429$	56.9%
$21/2_2^+$	3897.0	3688	$6402 \otimes 6429$	53.5%
$23/2_1^+$	3574.5	3487	$6402 \otimes 6429$	56.6%
$23/2_2^+$	4633.2	4519	$6312 \otimes 6429$	28.8%
			$5412 \otimes 6429$	38.4%
$25/2_1^+$	4273.8	4053	$6402 \otimes 6429$	56.8%
$25/2_2^+$	4733.8	4613	$5412 \otimes 6429$	36.4%
			$6312 \otimes 6429$	28.5%
$27/2_1^+$	5374.7	5366	$5412 \otimes 6429$	35.3%
			$6312 \otimes 6429$	30.6%
$27/2_2^+$	5748.3	5773	$5412 \otimes 6429$	60.8%
			$6312 \otimes 6429$	20.1%
$27/2_3^+$	6025.3	6348	$5412 \otimes 6429$	37.6%
			$6312 \otimes 6429$	38.7%
$13/2^-$	2120.7	1947	$6411 \otimes 6429$	64.2%
$15/2_1^-$	2150.2	1854	$6411 \otimes 6429$	60.3%
$15/2_2^-$	2491.7	2187	$6411 \otimes 6429$	66.4%
$17/2_1^-$	2160.0	2031	$6411 \otimes 6429$	66.2%
$17/2_2^-$	2597.2	2915	$6411 \otimes 6429$	65.6%
$17/2_3^-$	2896.6	3322	$6321 \otimes 6429$	35.8%
$19/2^-$	2927.3	2879	$6411 \otimes 6429$	68.0%
$21/2^-$	3717.6	3739	$5421 \otimes 6429$	40.6%
			$5403 \otimes 6429$	24.1%
$23/2^-$	4522.9	4590	$5421 \otimes 6429$	37.4%
			$5403 \otimes 6429$	28.0%
$25/2^-$	5493.6	5361	$5403 \otimes 6429$	61.6%
$29/2^-$	6239.9	6284	$5403 \otimes 6429$	64.5%
$31/2^-$	6827.2	6906	$5403 \otimes 6429$	63.9%
$33/2^-$	7500.5	7539	$5403 \otimes 6429$	63.1%

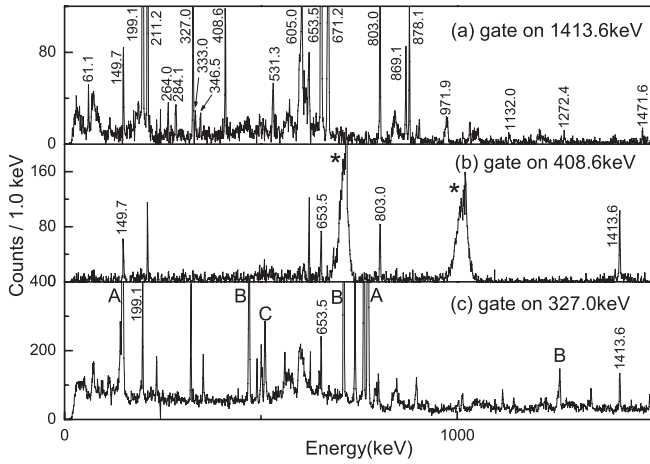


FIG. 8. Spectra of γ rays for ^{91}Mo , gated on (a) 1413.6 keV; (b) 408.6 keV; (c) 327.0 keV. Peaks labeled with asterisks, A, B and C in the spectra originate from the contaminations of ^{10}B [35], ^{92}Mo [34], ^{92}Nb [9], $e^+ + e^-$, respectively.

from the $p_{1/2}$ to the $g_{9/2}$ orbit, but for $17/2^-$, $\pi(f_{5/2}^5 p_{3/2}^4 p_{1/2}^2 g_{9/2}^3) \otimes \nu(p_{1/2}^2 g_{9/2}^9)$ contributes maximally.

V. THE SYSTEMATIC FEATURES WITH NEIGHBORING NUCLEI

Energies of several positive parity states for the $N=49$ odd-A isotones ^{89}Zr , ^{91}Mo , ^{93}Ru [21], ^{95}Pd [22], and odd-odd isotones ^{88}Y [17], ^{90}Nb [19], ^{92}Tc [21, 42], ^{94}Rh [21] are shown in Fig. 10. According to shell model calculations, these states in ^{88}Y , ^{89}Zr and ^{90}Nb mainly arise from $\pi(p_{1/2}^0 g_{9/2}^n)$ ($n=1, 2, 3$), but for the $J \geq 10\hbar$ states in the two odd-odd nuclei, proton excitations across the $Z=38$ subshell contribute significantly [17, 43, 44]. When it comes to other nuclei with $Z \geq 42$, the $\pi(p_{1/2}^2 g_{9/2}^n)$ ($n=2, 3, 4, 5, 6$) configurations dominate these states [21, 22]. The low-lying level structures of these odd-A isotones (or odd-odd isotones) are similar.

As illustrated in Fig. 10(a), the energy gap between the first excited state and the ground state for ^{89}Zr is about 0.5 MeV more than the others, which is influenced by the $Z=40$ subshell. It can be noted that with the increase of valence protons, the excitation energies for those yrast states decrease slowly. This may be because the valence protons become closer to the high- j $\pi g_{9/2}$ when the proton number increases and proton excitations become relatively easier. However, the difference for energies of the yrast $13/2^+$ states in ^{91}Mo , ^{93}Ru , and ^{95}Pd is quite small and the energies are close to that of the yrast 10^+ states in ^{92}Tc and ^{94}Rh . The energies of the yrast $17/2^+$ states are similar to the yrast 12^+ states as well, which indicates proton Fermi levels of these nuclei should be close. In Fig. 10(b), one sees the gap between the 10^+ and 8^+ states in ^{88}Y and ^{90}Nb is larger than that in ^{92}Tc and ^{94}Rh , probably because the yrast 10^+ states in the

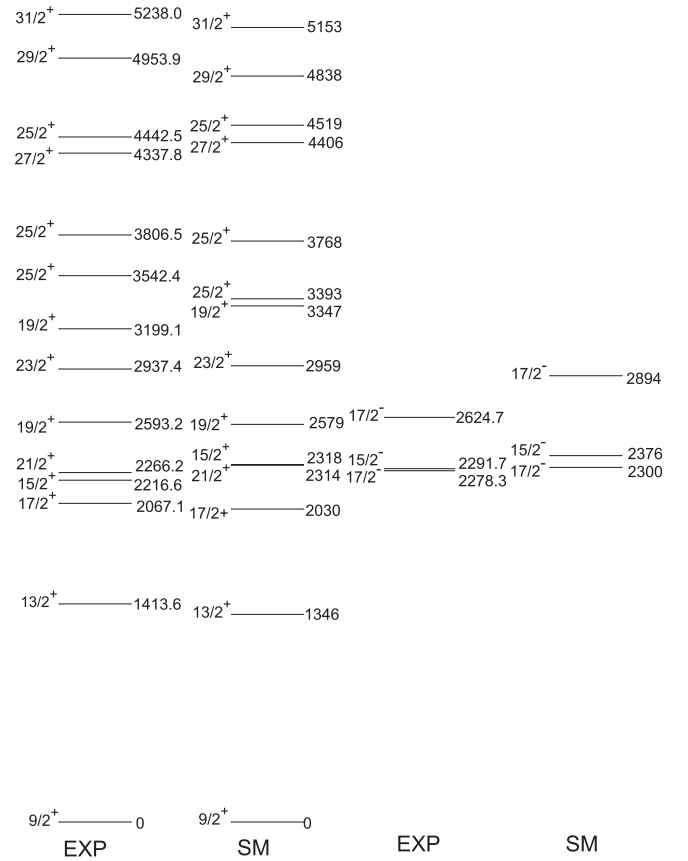


FIG. 9. Comparison of the calculated levels and the experimental levels of ^{91}Mo .

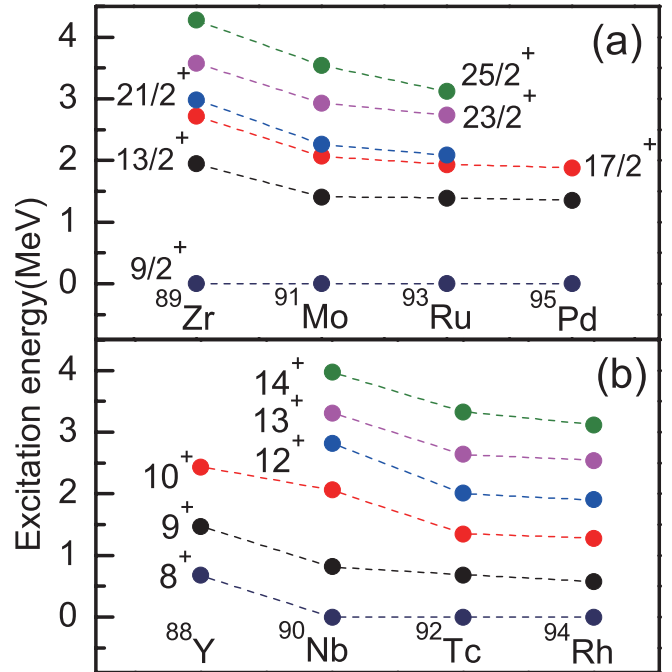


FIG. 10. (a) Comparison of the low-lying yrast states in the ^{89}Zr , ^{91}Mo , ^{93}Ru , ^{95}Pd [21, 22]; (b) The same as (a), but for ^{88}Y , ^{90}Nb , ^{92}Tc , ^{94}Rh [17, 19, 21, 42].

TABLE IV. Main components of the wave functions and their partitions in ^{91}Mo . $\pi \otimes \nu$ represents $\pi(f_{5/2}p_{3/2}p_{1/2}g_{9/2}) \otimes \nu(p_{1/2}g_{9/2})$.

J^π	E_{exp}	E_{cal}	Wave function	Partitions
\hbar	keV	keV	$\pi \otimes \nu$	
$9/2^+$	0	0	$6422 \otimes 29$	37.0%
			$6404 \otimes 29$	24.8%
$13/2^+$	1413.6	1346	$6422 \otimes 29$	31.3%
			$6404 \otimes 29$	23.4%
$15/2^+$	2216.6	2318	$6422 \otimes 29$	49.2%
			$6404 \otimes 29$	21.3%
$17/2^+$	2067.1	2030	$6422 \otimes 29$	27.3%
			$6404 \otimes 29$	25.7%
$19/2_1^+$	2593.2	2579	$6422 \otimes 29$	52.7%
			$6404 \otimes 29$	20.3%
$19/2_2^+$	3199.1	3347	$6422 \otimes 29$	20.5%
			$6404 \otimes 29$	23.1%
$21/2^+$	2266.2	2314	$6422 \otimes 29$	43.1%
			$6404 \otimes 29$	25.4%
$23/2^+$	2937.4	2959	$6422 \otimes 29$	44.8%
			$6404 \otimes 29$	25.7%
$25/2_1^+$	3542.4	3393	$6422 \otimes 29$	38.2%
			$6404 \otimes 29$	26.4%
$25/2_2^+$	3806.5	3768	$6404 \otimes 29$	20.6%
			$5414 \otimes 29$	42.7%
$25/2_3^+$	4442.5	4519	$6422 \otimes 29$	27.9%
			$5414 \otimes 29$	25.9%
$27/2^+$	4337.8	4406	$6404 \otimes 29$	26.4%
			$5414 \otimes 29$	33.5%
$29/2^+$	4953.9	4838	$6404 \otimes 29$	24.4%
			$5414 \otimes 29$	39.4%
$31/2^+$	5238.0	5153	$5414 \otimes 29$	73.6%
$15/2^-$	2291.7	2376	$6413 \otimes 29$	78.3%
$17/2_1^-$	2278.3	2300	$6413 \otimes 29$	74.1%
$17/2_2^-$	2624.7	2894	$6413 \otimes 29$	19.5%
			$5423 \otimes 29$	49.7%

VI. SUMMARY

High spin states of ^{89}Zr and ^{91}Mo were studied via the reactions $^6\text{Li}+^{89}\text{Y}$ at 34 MeV beam energy. The level structures of both nuclei have been extended. The spins for new levels were assigned based on their ADO ratios. Excited states of ^{89}Zr and ^{91}Mo have been interpreted in the framework of the spherical-basis shell model. The results indicate that the low lying states are dominated by particle excitations from the $\pi p_{1/2}$ orbit to the $\pi g_{9/2}$ orbit. With the increase of the excitation energy, the states are well described by proton excitations across the Z=38 subshell into higher orbits. Finally, we study the systematic features of N=49 isotones. With the increase of proton number, the valence protons becoming closer to the high-j $\pi g_{9/2}$ causes the decrease of the excitation energies for the same states.

VII. ACKNOWLEDGMENT

We are grateful to the INFN-LNL staff for providing stable ^6Li beam throughout the experiment. This work is supported by the National Natural Science Foundation of China (Grants No.12175086, No.11975040, No.U2167204 and No.U1867210), Guangdong Basic and Applied Basic Research Foundation (Grant No.2021B151520027) and the U.S. Department of Energy, Office of Science, Office of Nuclear Physics, under contract number DE-AC02-06CH11357.

-
- [1] Z. G. Wang, M. L. Liu, Y. H. Zhang, *et al.*, Phys. Rev. C **89**, 044308 (2014).
- [2] H.-W. Li, J.-B. Lu, G.-S. Li, *et al.*, Chinese Physics C **38**, 074004 (2014).
- [3] E. A. Stefanova, R. Schwengner, J. Reif, *et al.*, Phys. Rev. C **62**, 054314 (2000).
- [4] C. J. Xu, S. Y. Wang, C. Y. Niu, *et al.*, Phys. Rev. C **86**, 027302 (2012).
- [5] A. Bödeker, K. P. Lieb, C. J. Gross, *et al.*, Phys. Rev. C **48**, 1617 (1993).
- [6] E. K. Warburton, J. W. Olness, C. J. Lister, *et al.*, Phys. Rev. C **31**, 1184 (1985).
- [7] T. Hori, T. Masue, A. Odahara, *et al.*, Phys. Rev. C **80**, 034306 (2009).
- [8] G. García-Bermúdez, M. A. Cardona, R. V. Ribas, *et al.*, Phys. Rev. C **48**, 1623 (1993).
- [9] Y.-F. Lv, J.-B. Lu, G.-L. Zhang, *et al.*, Chinese Physics C **43**, 104102 (2019).
- [10] P. Singh, R. G. Pillay, J. A. Sheikh, and H. G. Devare, Phys. Rev. C **45**, 2161 (1992).
- [11] S. Saha, R. Palit, J. Sethi, *et al.*, Phys. Rev. C **86**, 034315 (2012).
- [12] Z. Q. Li, S. Y. Wang, C. Y. Niu, *et al.*, Phys. Rev. C **94**, 014315 (2016).
- [13] S. S. Ghugre and S. K. Datta, Phys. Rev. C **52**, 1881 (1995).
- [14] Y. Wakabayashi, T. Fukuchi, Y. Gono, *et al.*, Journal of the Physical Society of Japan **76**, 114202 (2007).
- [15] Y. Zheng, Y. H. Wu, X. G. Wu, *et al.*, Phys. Rev. C **100**, 014325 (2019).
- [16] G. Rainovski, R. Schwengner, K. D. Schilling, *et al.*, Phys. Rev. C **65**, 044327 (2002).
- [17] M. Bunce, P. H. Regan, V. Werner, *et al.*, Phys. Rev. C **87**, 044337 (2013).
- [18] A. Chakraborty, Krishichayan, S. S. Ghugre, *et al.*, Phys. Rev. C **72**, 054309 (2005).
- [19] X. Z. Cui, L. H. Zhu, X. G. Wu, *et al.*, Phys. Rev. C **72**, 044322 (2005).
- [20] S. Ray, N. S. Pattabiraman, R. Goswami, *et al.*, Phys. Rev. C **69**, 054314 (2004).

- [21] S. E. Arnell, D. Foltescu, H. A. Roth, *et al.*, Phys. Rev. C **49**, 51 (1994).
- [22] R. Mărginean, C. Rusu, N. Mărginean, D. Bucurescu, *et al.*, Phys. Rev. C **86**, 034339 (2012).
- [23] A. Nilsson and M. Grecescu, Nuclear Physics A **212**, 448 (1973).
- [24] E. K. Warburton, J. W. Olness, C. J. Lister, *et al.*, Journal of Physics G: Nuclear Physics **12**, 1017 (1986).
- [25] S. Saha, R. Palit, J. Sethi, *et al.*, Phys. Rev. C **99**, 054301 (2019).
- [26] P. Singh, R. G. Pillay, J. A. Sheikh, and H. G. Devare, Phys. Rev. C **48**, 1609 (1993).
- [27] Z. Huang, G. X. Zhang, S. P. Hu, *et al.*, The European Physical Journal A **57**, 137 (2021).
- [28] A. Goasduff, D. Mengoni, F. Recchia, *et al.*, Nuclear Instruments and Methods in Physics Research Section A: Accelerators, Spectrometers, Detectors and Associated Equipment **1015**, 165753 (2021).
- [29] D. Testov, D. Mengoni, A. Goasduff, *et al.*, The European Physical Journal A **55**, 47 (2019).
- [30] S. Hu, G. Zhang, G. Zhang, *et al.*, Nuclear Instruments and Methods in Physics Research Section A: Accelerators, Spectrometers, Detectors and Associated Equipment **914**, 64 (2019).
- [31] M. Piiparinen, A. Ata, J. Blomqvist, *et al.*, Nuclear Physics A **605**, 191 (1996).
- [32] Y. H. Zhang, M. Hasegawa, W. T. Guo, *et al.*, Phys. Rev. C **79**, 044316 (2009).
- [33] B. Singh, Nuclear Data Sheets **114**, 1 (2013).
- [34] N. S. Pattabiraman, S. N. Chintalapudi, S. S. Ghugre, *et al.*, Phys. Rev. C **65**, 044324 (2002).
- [35] F. Ajzenberg-Selove, Nuclear Physics A **490**, 1 (1988).
- [36] M. Honma, T. Otsuka, T. Mizusaki, and M. Hjorth-Jensen, Phys. Rev. C **80**, 064323 (2009).
- [37] B. Brown and W. Rae, Nuclear Data Sheets **120**, 115 (2014).
- [38] A. Hosaka, K.-I. Kubo, and H. Toki, Nuclear Physics A **444**, 76 (1985).
- [39] X. Ji and B. H. Wildenthal, Phys. Rev. C **37**, 1256 (1988).
- [40] D. Gloeckner, Nuclear Physics A **253**, 301 (1975).
- [41] F. Serduke, R. Lawson, and D. Gloeckner, Nuclear Physics A **256**, 45 (1976).
- [42] S. S. Ghugre, S. B. Patel, and R. K. Bhowmik, Phys. Rev. C **51**, 1136 (1995).
- [43] P. C. Srivastava, V. Kumar, and M. J. Ermamatov, Physics of Atomic Nuclei **77**, 1334 (2014).
- [44] W. Yi-Heng, Y. Dong, M. Ke-Yan, and L. Peng-Wei, Nukleonika **64**, 113 (2019).